
Article:
Peterson, R.C., Jimack, P.K. and Kelmanson, M.A. (2001) On the stability of viscous free-surface flow supported by a rotating cylinder. Proceedings of the Royal Society Series A: Mathematical, Physical and Engineering Sciences, 457 (2010). pp. 1427-1445. ISSN: 1471-2946

https://doi.org/10.1098/rspa.2000.0780

On the stability of viscous, free-surface flow supported by a rotating cylinder

By R.C. Peterson[1,2], P.K. Jimack[1] and M.A. Kelmanson[2]†

[1]*School of Computing/*[2]*Department of Applied Mathematics, University of Leeds, Leeds LS2 9JT, UK*

Using an adaptive finite-element (FE) scheme developed recently by the authors, we shed new light on the long-standing fundamental problem of the unsteady free-surface Stokes flow exterior to a circular cylinder rotating about its horizontal axis in a vertical gravitational field. For supportable loads, we observe that the steady state is more readily attained for near-maximal fluid loads on the cylinder than for significantly sub-maximal loads. For the latter, we investigate large-time dynamics by means of a finite-difference (FD) approximation to the thin-film equations, which is also used to validate the adaptive finite element simulations (applied to the full Stokes equations) for these significantly sub-maximal loads. Conversely, by comparing results of the two methods, we assess the validity of the thin-film approximation as either the load is increased or the rotation rate of the cylinder is decreased. Results are presented on the independent effects of gravity, surface tension and initial film thickness on the decay to steady state. Finally, new numerical simulations of load shedding are presented.

Keywords: Viscous fluid mechanics, free-surface flow, Stokes approximation, finite-element methods, adaptive meshing

1. Introduction

The phenomenon of gravity-influenced, free-surface viscous flow exterior to a rotating cylinder — the supported-load problem — has been the subject of numerous investigations of diverse natures, e.g., experimental (Moffatt 1977, Joseph & Preziosi 1987, Kelmanson 1995), computational (Hansen & Kelmanson 1994), and theoretical (Pukhnachev 1977, Moffatt 1977, Preziosi & Joseph 1988, Kelmanson 1995, Duffy & Wilson 1999). Campanella & Cerro (1984) consider a related flow exterior to a rotating cylinder for the case when the cylinder is partially submerged in a bath of viscous fluid and Weidner *et al.* (1977) and Oron *et al.* (1977) consider gravity-driven flows exterior to a stationary cylinder.

Whilst we presently consider only the "coating-flow" problem, the closely related "rimming-flow" problem (interior to a rotating cylinder) has also been considered by many authors, e.g., Preziosi & Joseph (1988), Johnson (1988), Johnson (1990), Melo (1993), Wilson & Williams (1997) and Hosoi & Mahadevan (1999). Whilst rimming flows will not be considered further herein, the volume of literature on such flows bears witness to the fundamental scientific (and industrial) importance of the general area.

† Corresponding author, email mark@amsta.leeds.ac.uk

In the cited computational and theoretical treatises, the flow is assumed to be so viscous that the Stokes approximation can be used. Three-dimensional and time-dependent effects in coating flows are investigated by: Moffatt (1977) (whose laboratory experiments demonstrate azimuthal variations in the film thickness under certain conditions); Joseph & Preziosi (1987) (who perform experiments on bicomponent flows of immiscible liquids); Preziosi & Joseph (1988) (who perform experiments for both coating and rimming flows and consider axial flow variation theoretically); Weidner *et al.* (1997) (who solve the thin-film equations using an alternating-direction-implicit finite-difference algorithm); Oron *et al.* (1997) (who reduce the full governing equations to a simplified (set of) evolution equation(s)).

With the exception of Hansen & Kelmanson (1994) in the cited literature, previous studies of flows exterior to rotating cylinders have invoked a thin-film approximation at some stage in their analyses. In certain cases (e.g. Kelmanson 1995, Duffy & Wilson 1999) the free-surface thicknesses considered are of magnitude of the same order as the cylinder radius but still yield good results beyond their expected range of validity. To deal with a flow of arbitrary thickness, Weidner *et al.* (1997) note that numerical solution of the full set of equations is "difficult to implement and computationally intensive". However, in the present work, we use a new adaptive finite-element method (Peterson *et al.* 1999; Peterson 2000) in order to investigate time-dependent coating flows using the full Stokes approximation. As such, we are able to incorporate radial pressure gradients when the film thickness lies beyond the validity of thin-film theory. Indeed, investigation of such validity constitutes an important component of the present study.

Whilst the coating-flow phenomenon is demonstrable via the simplest of experiments — the rotation of a wooden spoon, its axis horizontal, previously dipped into syrup — the mathematics of the competing aspects of viscosity, surface tension and gravity precludes an explicit analytical solution except in those cases where the viscous fluid layer thickness (non–dimensionalized with respect to the cylinder radius) can be considered sufficiently small for thin-film theory to be invoked. Under such circumstances, one can estimate (Moffatt 1977; Kelmanson 1995) *maximum–supportable loads* (MSLs) as a function of the angular velocity of the cylinder, based upon the assumption that the flow is *steady*, i.e., should the angular velocity fall below a critical value, no steady solution exists and the fluid drains off. The iterative boundary-integral technique of Hansen & Kelmanson (1994) provides both two-dimensional Stokes-flow solutions and estimates for the MSL well beyond the thin-film regime — specifically, for film thicknesses of the order of the cylinder radius. This demonstrates that a full understanding of this simple-to-state problem is beyond the scope of analysis alone; further, it motivates the development of more sophisticated numerical approaches.

In § 2 (a) we review past and present assumptions in modelling the problem, and a Stokes-flow formulation is presented in § 2 (b). For the sake of completeness, we present in § 3 a brief outline of the authors' novel numerical method used throughout this paper: a time-dependent, adaptive, finite-element technique (Peterson *et al.* 1998, 1999; Peterson 2000) for solving a wide range of two-dimensional, free-surface, Stokes-flow problems in which there occurs the possibility of large variations in both domain geometry and free-surface curvature. Our method is quasi-time-dependent insofar as it solves the Stokes approximation at each time-step, time dependence being included via the kinematic boundary condition.

The principal aim of the present work is to investigate unsteady flows using the full Stokes equations, i.e. free from the potential constraint of any thin-film approximation. These comprise both stable (yet oscillatory) flows decaying to a steady state and unstable flows portending load shedding. Such stable and unstable flows are discussed in §§ 4 (a) and 4 (b) respectively. Furthermore, in § 4 (a), we attempt to quantify, using our full Stokes simulations, the concept of a thin film in the sense of whether, for particular choices of parameters, the lubrication approximation gives results which are comparable with those of our new method. A combination of the Stokes equations and Pukhnachev's (1977) lubrication approximation are then used to investigate the transient behaviour of stable films over a wide range of time scales. In § 4 (b) we present illustrations of the phenomena of lobe formation and load shedding which ensue when the MSL is exceeded. Although the present model considers only two-dimensional flow, these lobes bear striking similarity to the profiles of the three-dimensional lobes photographed in Moffatt's (1977) laboratory experiments over two decades ago. Brief conclusions are presented in § 5.

2. Formulation

(*a*) *Preliminary assumptions*

We consider the flow within a layer of incompressible viscous fluid of density ρ and dynamic viscosity μ exterior to an infinite circular cylinder of radius a rotating anticlockwise about its horizontal axis with angular velocity ω in a gravitational field $\boldsymbol{g} = -g\hat{\boldsymbol{j}}$, where $\hat{\boldsymbol{j}}$ is a unit vector aligned with the positive $y-$axis and g is the acceleration due to gravity. Two-dimensional Cartesian coordinates $x,\ y$ and (radial/transverse) polar coordinates $r,\ \theta$ centred on the cylinder axis are employed, and $\boldsymbol{r} = (x, y)$ denotes the position vector of a fluid particle.

The solutions computed herein indicate that the pattern of flow observed shows signs of rigid-body rotation, significant differences arising only in the case of large supported loads. Thus the present full Stokes approximation is consistent with both the numerics of Hansen & Kelmanson (1994) and theories of Preziosi & Joseph (1988) and Kelmanson (1995). In a rigid-body flow the velocity field takes the form

$$\boldsymbol{u} = -\omega\,\hat{\boldsymbol{r}} \times \hat{\boldsymbol{k}} = -\omega y\,\hat{\boldsymbol{\imath}} + \omega x\,\hat{\boldsymbol{j}},$$

where $\hat{\boldsymbol{k}} = \hat{\boldsymbol{\imath}} \times \hat{\boldsymbol{j}}$, $\hat{\boldsymbol{\imath}}$ and $\hat{\boldsymbol{j}}$ being respectively unit vectors in the positive x- and y-directions. In the absence of gravity, and provided the pressure is everywhere constant, any rigid-body motion (translation and/or rotation) is a solution of the Stokes equations. When surface tension is present the free surface will have minimal surface energy only when it is circular in profile; then, any configuration with circular cross-section (not necessarily concentric with the enclosed cylinder) rotating with uniform angular velocity will be an exact solution of the Stokes equations (but only in the absence of gravity). In these circumstances the everywhere-constant pressure p is that required to satisfy the condition of continuity of normal stress at the free surface. In the presence of gravity $\boldsymbol{g}$, the assumption of a rigid-body motion of the fluid results in the governing equations being reduced to

$$\boldsymbol{\nabla} p = \rho \boldsymbol{g},$$

the solution of which is simply $p = p_0 + \rho g y$ so that p cannot be constant and the conclusion must be drawn that an exact rigid-body rotation in Stokes flow is not possible in the presence of a gravitational field.

After Hansen & Kelmanson (1994), we non-dimensionalize the Navier-Stokes equations using velocity, time and stress scales $a\omega$, ω^{-1} and $\mu\omega$ respectively to obtain

$$Re\left[\frac{\partial \boldsymbol{u}^*}{\partial t^*} + (\boldsymbol{u}^* \cdot \boldsymbol{\nabla}^*)\boldsymbol{u}^*\right] = \Delta^* \boldsymbol{u}^* - \boldsymbol{\nabla}^* p^* - \gamma \hat{\boldsymbol{j}}, \tag{2.1}$$

where the Reynolds number Re is given by

$$Re = \frac{\rho a^2 \omega}{\mu},$$

the Stokes number γ — the dimensionless acceleration due to gravity — is given by

$$\gamma = \frac{\rho g a}{\omega \mu},$$

and the superscripts $(^*)$ denote dimensionless physical variables. The inertial terms in equation (2.1) are therefore dominated by the gravitational term if the Galileo number $g/a\omega^2 \gg 1$. Hansen & Kelmanson (1994) calculate $Re \sim O(10^{-1})$ for an apparatus similar to that described by Moffatt (1977) and a value of $\gamma \simeq 1$: accordingly, $g/a\omega^2 \sim O(10)$ and the validity of the Stokes approximation is confirmed.

(*b*) *Stokes-flow model*

The simplest initial condition, and the one adopted here, is the enforcement of a circular free-surface profile coaxial with the rotating cylinder. Thus the initial condition is specified by a single parameter, the mean film thickness $\bar{h}^* = \bar{h}/a$. Alternatively, one may specify the non-dimensional cross-sectional area or load Λ^*, given by

$$\Lambda^* = \pi\left(\left(1 + \bar{h}^*\right)^2 - 1\right).$$

In the limit $Re \to 0$, (2.1) reduces to

$$\Delta^* \boldsymbol{u}^* - \boldsymbol{\nabla}^* p^* - \gamma \hat{\boldsymbol{j}} = \boldsymbol{0}, \tag{2.2}$$

which must be solved together with the continuity equation

$$\boldsymbol{\nabla}^* \cdot \boldsymbol{u}^* = 0. \tag{2.3}$$

The boundary condition on the cylinder is

$$\boldsymbol{u}^* = -\sin\theta\, \hat{\boldsymbol{i}} + \cos\theta\, \hat{\boldsymbol{j}} \tag{2.4}$$

and the free-surface stress is

$$\boldsymbol{f} = -\sigma k \hat{\boldsymbol{n}} \tag{2.5}$$

where k is the curvature of the free surface, $\hat{\boldsymbol{n}}$ is the outward free-surface normal, and σ is the coefficient of surface tension. On non-dimensionalization equation (2.5) becomes

$$\boldsymbol{f}^* = -\frac{\alpha}{R_c^*}\hat{\boldsymbol{n}}, \tag{2.6}$$

where R_c^* is the dimensionless free-surface radius of curvature and

$$\alpha = \frac{\sigma}{a\mu\omega}$$

is the inverse capillary number (a dimensionless measure of surface tension). The kinematic boundary condition at the free surface is

$$\hat{\boldsymbol{n}} \cdot \boldsymbol{u}^* = \hat{\boldsymbol{n}} \cdot \dot{\boldsymbol{s}}^*, \tag{2.7}$$

where $\boldsymbol{s}^*$ is the location of a point on the free surface and a superior dot indicates a temporal derivative.

The calculations of Hansen & Kelmanson (1994) demonstrate that the free-surface profiles are only very weakly dependent upon the surface tension: e.g., an experiment is reported in which, for $\gamma = 1$ and a flux of $\psi_\infty^* = 0.9$ (see equations (2.8) and (2.9) below), the maximum steady-state non-dimensional free-surface elevation (at $\theta = 0$) reduces from 0.608 to 0.599 when α is increased from 0 to (an unrealistically large) 100. Furthermore, they prove that, when $\alpha = 0$, perfect symmetry in geometry is expected about $y = 0$ *however great the (supportable) load* in the steady flow; Moffatt (1977) discovered this symmetry theoretically in the thin-film case. Near-symmetry of the free surface is apparent even when the surface tension is (unrealistically) large, e.g. when $\alpha = 100$; $\alpha = 2$ might be a more appropriate value for the experiments in Moffatt (1977). Bearing these observations in mind, a value of $\alpha = 1$ was used throughout the current investigations, unless otherwise stated. The formulation is completed by specification of both Λ^* and γ.

Hansen & Kelmanson (1994) employ a stream-function formulation in which the dimensionless steady-state flux ψ_∞^* (independent of θ) is *prescribed*, whereafter a non-gradient optimization procedure is used to locate the steady free surface for which the flux is ψ_∞^*. In the time-dependent case, however, the flux will vary with both θ and t according to

$$\psi^*(\theta,t) = -\int_{r^*=1}^{r^*=1+h^*(\theta,t)} \boldsymbol{u}^*(\theta,t)\cdot(-\sin\theta\,\hat{\boldsymbol{i}} + \cos\theta\,\hat{\boldsymbol{j}})\,dr, \tag{2.8}$$

where $h^*(\theta,t)$ is the dimensionless film thickness and the integral is evaluated along the extension of a radius of the cylinder. Then clearly

$$\lim_{t\to\infty} \psi^*(\theta,t) = \psi_\infty^*. \tag{2.9}$$

Our finite-element method requires specification of an initial condition of the form $h^*(\theta,0) = h_0^*(\theta)$, a known function of θ. Therefore, if we wish to compare our large-time results with those of Hansen & Kelmanson (1994) we are faced with the problem of specifying *a priori* the precise $h_0^*(\theta)$ which develops into the $h^*(\theta,t)$ in (2.8) which in turn yields a $\psi^*(\theta,t)$ in (2.8) which, as $t \to \infty$, tends to the

prescribed value of ψ^*_∞ on the right-hand side of (2.9). Thus, in the absence of a highly (indeed, excessively) computationally intensive search, results from our time-dependent scheme do not admit direct comparison with those arising from specific parameter values used in Hansen & Kelmanson (1994).

In the present iterative approach, the initial free-surface profile need be specified only approximately. As such, gravity can be neglected in specifying the approximate dimensionless initial flux, from which a dimensionless initial mean film-thickness $\bar{h}^*$ can be specified. Hereafter all superscripts will be dropped, and the symbols $\boldsymbol{u}$, p, $\boldsymbol{f}$, h, $\bar{h}$, Λ and t will subsequently refer to the corresponding dimensionless quantities.

3. Adaptive numerical method

The numerical scheme used here is an Eulerian primitive-variable finite-element method, applied on a continuously deforming grid which follows the evolution of the domain in which the fluid lies as the free surface evolves. The boundary of this domain is represented as a fixed part (the surface of the cross-section of the cylinder) and a free-surface part, the location of which is allowed to change due to the kinematic boundary condition (2.7). At each time-step the solution of equations (2.2) to (2.4) and (2.6) provides the corresponding instantaneous flow within this domain. Full details of the algorithms may be found in Peterson *et al.* (1999) and Peterson (2000). It should be noted that the explicit scheme employed to update the location of the free surface does not enforce mass conservation. Since a primary aim of this work is to investigate the sensitive free-surface dynamics leading up to load shedding, we use only the kinematic boundary condition (2.7) to update the free surface at each time-step. Measurement of any change in the mass of fluid thus provides an automatic check on the validity of solutions obtained.

For the numerical simulations undertaken in this work the location of the free-surface is updated explicitly at each time-step using a simple first-order discretization of (2.7). The interior mesh is then updated so as to reflect the deformation of the boundary. For the preliminary investigations we used a linear elasticity model, as suggested by Lynch (1982); for the later (unstructured-mesh) calculations we also used Jacobi smoothing (Peterson *et al.* 1999; Peterson 2000). For the generation of the initial mesh use is made of the mesh generator *Triangle* (Shewchuk 1996), which is able to generate a Delaunay triangulation of a region given a discretization of the boundary. Before the start of each time-step the quality of the existing mesh is assessed and, when necessary, the boundary discretization is either refined or coarsened and the interior mesh regenerated (again using *Triangle*).

Once the update of the boundary and interior mesh has taken place it is then necessary to compute the values of the flow variables $\boldsymbol{u}$ and p on the new mesh. In order to allow the natural stress boundary condition (2.6) to be imposed within the finite element model it is necessary to rewrite the Stokes equation (2.2) in stress-divergence form

$$\Delta\boldsymbol{u} + \boldsymbol{\nabla}(\boldsymbol{\nabla}\cdot\boldsymbol{u}) - \boldsymbol{\nabla}p - \gamma\hat{\boldsymbol{j}} = \boldsymbol{0}.$$

The corresponding weak form is then such that the free-surface stress $\boldsymbol{f}$ is explicitly present in the boundary integrals that arise when the Galerkin method is employed (Gresho 1991; Peterson *et al.* 1999; Peterson 2000). In order to ensure a stable discretization of this weak form we use the Galerkin method with a piecewise-quadratic

Mesh	N_θ	N_r	Elements	Unknowns
I	32	5	256	1184
II	64	5	512	2368
III	128	5	1024	4736
IV	64	3	256	1216
V	64	9	1024	4672
VI	64	7	768	3520

Table 1. *Mesh statistics used in simulations of stable flows.*

representation of each velocity component and a piecewise-linear representation of the pressure (Gunzburger 1989). The use of isoparametric mappings for the elements adjacent to the free surface allows a piecewise-quadratic representation of the free surface to be maintained (Strang & Fix 1973; Ciarlet 1978; Peterson 2000).

Having updated the boundary and the mesh, and formed the mixed finite element equations at each time-step, it now remains to solve these simultaneous linear equations in order to determine approximations to $\boldsymbol{u}$ and p. These equations are sparse, symmetric and indefinite and so it is appropriate to use an iterative technique such as the Conjugate Residual method (Ramage & Wathen 1994; Ashby *et al.* 1990). For improved efficiency this is preconditioned using an incomplete LU (ILU) factorization of the system matrix (Saad 1996). Since the ILU factorization is used only as a preconditioner then, even though the system matrix will change at each time-step, the factorization can be reused for a number of steps without a significant deterioration in its performance as a preconditioner.

In the investigations which follow in § 4 (a) the evolution of the free-surface profile is such that boundary refinement or coarsening is unnecessary. Hence the connectivity of the initial mesh remains unaltered throughout the entire simulation (although the mesh itself evolves with time). In order to demonstrate the mesh independence of our solutions, a number of different meshes of fixed connectivity were employed. These meshes contained N_θ elements in the circumferential direction and N_r elements in the radial direction: see table 1 for details.

For all experiments in § 4 (a), a fixed time-step of length $\delta t = 0.005$ was employed. That such a relatively large time-step could be used appears to reflect the fact that the normal component of the free-surface velocity is here typically small. The ILU preconditioner, recomputed every ten time-steps, yielded an incomplete factorization with 2–4 times the number of entries as the original sparse system matrix; consequently, it is relatively cheap to apply. All linear systems were solved to an absolute tolerance of 10^{-10}, and convergence of numerical results with decreasing mesh size (in both the radial and transverse direction) and decreasing time-step was established by performing calculations using a variety of meshes selected from table 1.

Finally, we note that the present primitive-variable FE method is more versatile than that of the boundary-integral method (BIM) of Hansen & Kelmanson (1994) which employs an optimization/biharmonic-stream-function formulation which is ideally suited to the consideration of steady-state problems. Not only is our FE method time-dependent, but it can also be readily modified to accommodate (extreme) changes in geometry (Peterson *et al.* 1999; Peterson 2000) whereas the Green's functions used in the BIM are applicable only to a specific geometry. More-

over, the FE method is more robust for problems involving disparate magnitudes of free-surface curvatures, such as those which arise in § 4 (b).

4. Results and discussion

Leading-order thin-film theory (Moffatt 1977), the boundary-integral technique (Hansen & Kelmanson 1994) and leading-and-first-order thin-film theory (Kelmanson 1995) independently establish that the maximum-supportable load decreases monotonically with the Stokes number γ. Hansen & Kelmanson (1994) report that their (steady-state) solver invariably located a steady-state solution for loads less than the maximum supportable. For loads greater than this they found no steady solution. In those cases where steady states were found, their method gives no means of determining the *rate* at which this might be approached from given initial conditions.

With these two distinct flow types in mind, we present the results of our unsteady-flow investigations in two categories: first, in § 4 (a), stable solutions, the large-time properties of which can be compared with steady-state results in the literature; second, in § 4 (b), unstable flows — never before simulated numerically using the full Stokes approximation — in which load shedding, leading to breakup of the solution domain, occurs. The dual nature of the solutions discovered in our numerical experiments is most clearly summarized in figure 1, which is discussed in more detail in §§ 4 (a) and (b).

(*a*) *Stable flow: effect of parameters on decay to steady state*

At those points denoted by + in figure 1, we computed a free surface for which the film thickness $h(\theta, t)$ is an oscillatory function of t, the amplitude of the oscillation displaying an observable decay with t over the first fifty cylinder rotations. Such behaviour, which arises naturally in the present solution of the Stokes equations, is consistent with the thin-film computations of Moffatt (1977), who first added weak diffusion in the θ direction, the precise form of which is given by Pukhnachev (1977). For example, with $\{\Lambda, \gamma\} = \{1.3, 12.5\}$, the oscillation amplitude decayed (by $t = 300$) from approximately 32 to 2 per cent of the mean film thickness of 0.236. Similarly, with $\{\Lambda, \gamma\} = \{1.2, 12.5\}$, the oscillation amplitude decayed from approximately 25 to 5 per cent of the mean film thickness of 0.210 over the same period of time. Since these parameters give sub-maximal-load positions in $\{\Lambda, \gamma\}$ parameter space, convergence to the steady state was expected, but the observation that *reducing* Λ led to *slower* convergence was not. Interestingly, the solutions found to be the most stable (in the sense that the oscillations decayed the most rapidly) were those which were closest (in $\{\Lambda, \gamma\}$ parameter space) to the *maximal* supported loads found by Hansen & Kelmanson (1994). Further, by reducing Λ sufficiently, i.e. at those points denoted by $\diamond$ in figure 1, no observable decay of the amplitude of the oscillations in $h(\theta, t)$ could be detected within the first fifty rotations of the cylinder, $t \simeq 300$.

To investigate $t > O(1000)$ large-time behaviour it is apparent that the computational cost of the finite-element method for the full Stokes problem is prohibitive. Pursuing detailed suggestions from Hinch (2000, personal communication) we therefore considered the lubrication approximation. Specifically, a fourth-order central

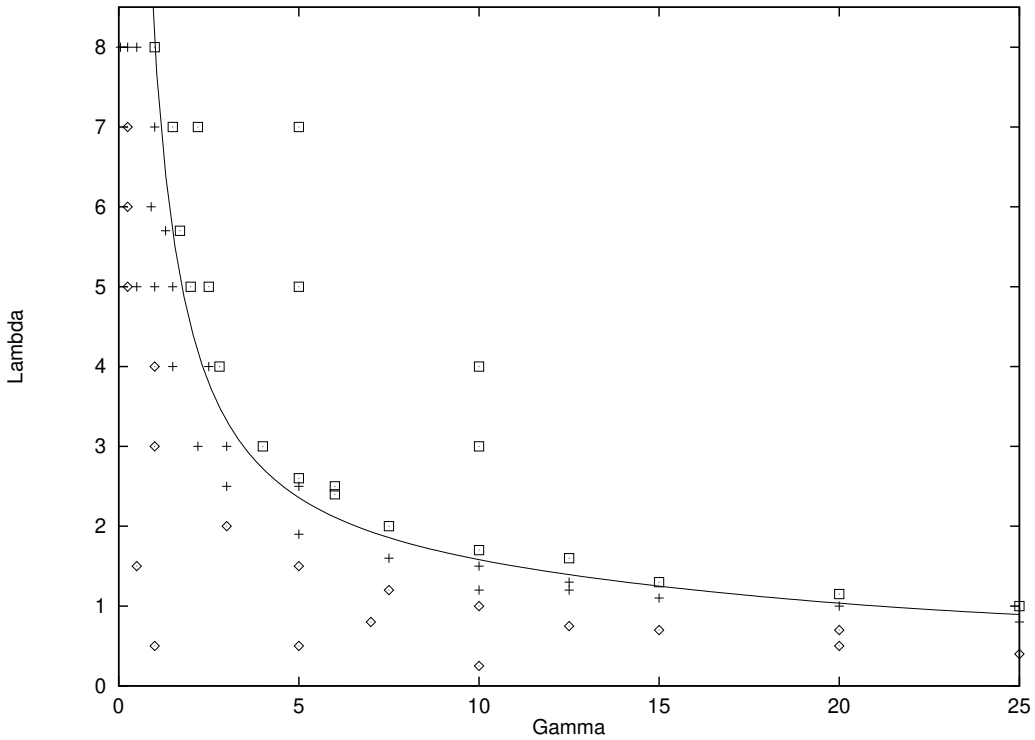

Figure 1. Solution types in $\{\Lambda, \gamma\}$ parameter space, relative to least-squares fit (solid line) to maximum-supportable load data of Hansen & Kelmanson (1994): + stable, decay to steady state evident at $t = 300$; $\diamond$ stable, no sign of decay to steady state at $t = 300$; $\square$ unstable. $\alpha = 1$ in all cases.

difference scheme with explicit time-stepping was applied to the equation for $h(\theta, t)$ given by Pukhnachev (1977),

$$h_t + \left(h - \frac{\gamma}{3}h^3\cos\theta\right)_\theta + \frac{\alpha}{3}\left(h^3\left(h_{\theta\theta} + h\right)_\theta\right)_\theta = 0, \tag{4.1}$$

using the initial condition $h(\theta, 0) = h_0$, a constant. We note in passing that the steady-state asymptotic solution as $h_0 \to 0^+$, $h_\infty(\theta)$, of this initial-value problem,

$$h_\infty(\theta) = h_0 + \frac{\gamma}{3}h_0^3\cos\theta + \frac{\gamma^2}{6}h_0^5\cos 2\theta + O(h_0^7, \alpha h_0^8),$$

is the solution about which our observed time-dependent numerical solutions oscillate in this thin-film limit.

We investigated the extent to which (4.1) is applicable, employing our finite-element solutions as a guide. As can be seen from figure 2, which shows a comparison between results of the lubrication approximation (4.1) and the Stokes equation (2.2) for increasing h_0, there is a noticeable deviation for an initial film thickness which is approximately 15% of the cylinder radius when $\gamma = 12.5$ and $\alpha = 1$. Figure 3 reveals that, when γ is reduced to unity, the lubrication approximation appears to be acceptable for an initial film thickness of at least 40% of the cylinder radius.

Thus, the physical characteristics of the fluid and roller remaining fixed, we infer that either reducing the gravitational field or increasing the rotation rate gives rise to a situation where the thin-film approximation is increasingly vindicated, despite the increasingly thick layer of fluid that is supportable.

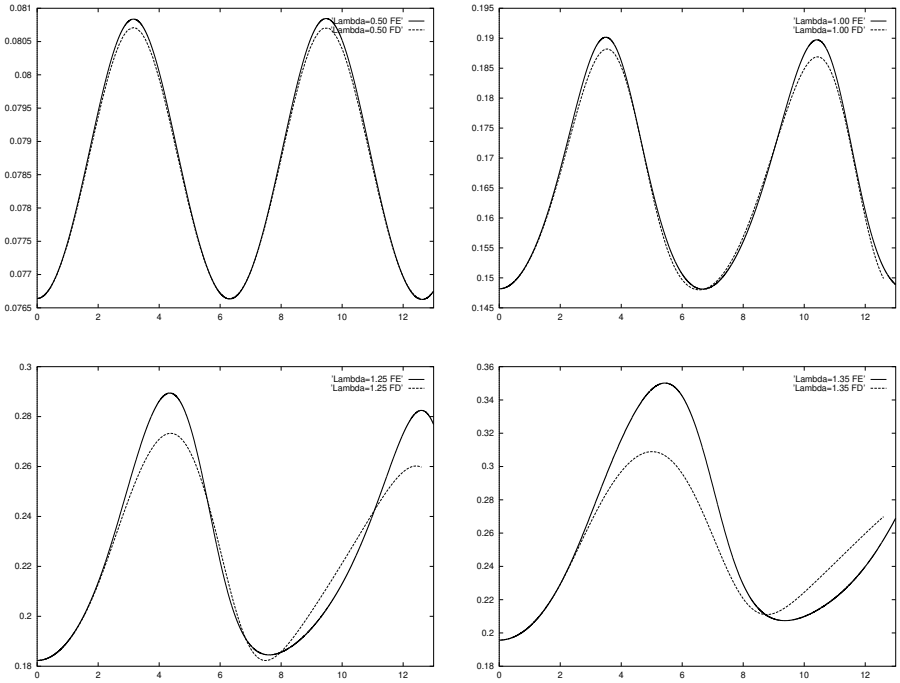

Figure 2. $h(0,t)$ as calculated by the FE solution of Eq. (2.2) (solid line) and FD solution of Eq. (4.1) (dashed line). $\alpha = 1$ and $\gamma = 12.5$ throughout and, from left to right and top to bottom, $\Lambda = 0.50,\ 1.00,\ 1.25,\ 1.35$ (i.e. $h_0 = 0.077,\ 0.148,\ 0.182,\ 0.195$).

Recalling our observation that, as $\Lambda \to 0^+$, the amplitude of the oscillations in the solution of the Stokes approximation appeared not to decay even by $t = 300$, we computed $h(0,t)$ from (4.1) (taking $h_0 = 0.11,\ \gamma = 12.5,\ \alpha = 1$). Figure 4 shows that an intial decline occurs in *both* the (normalized) maximum and minimum values of $h(0,t)$ up to $t \simeq 200$. This dual decline implies no reduction in the amplitude of the oscillations and might reasonably be attributed to numerical dissipation inherent in the finite-difference scheme. This impression is compounded by the fact that the magnitude of the dissipative term in (4.1) is comparable to that of the local truncation error of the fourth-order scheme. However, continuing the integration up to $t = 2000$ demonstrates beyond doubt that decay of such oscillations (of the thin-film approximation) does indeed eventually occur.

We find that this decay occurs for a range of initial film thicknesses h_0, and that the thinner the film, the smaller is the rate of this decay *and* the longer is the delay before it occurs: this observation is confirmed in figure 5, which shows the dependence of $h(0,t)$ on h_0 for $\alpha = 1$ and $\gamma = 12.5$. This is a result of significant physical interest, bearing in mind the importance of roller-coating technology in industrial processes. From a practical point of view we have demonstrated that, if

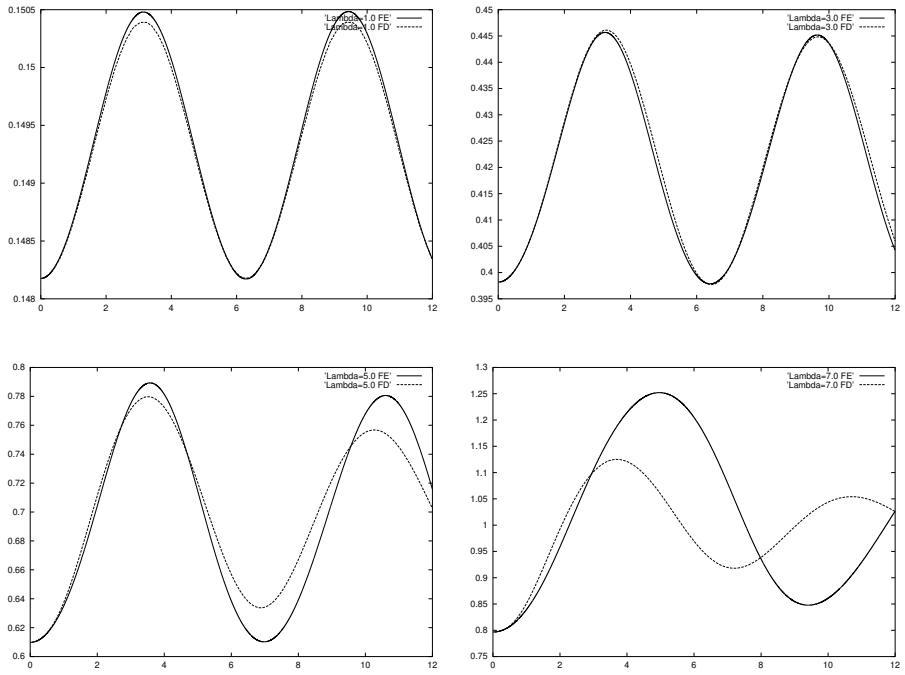

Figure 3. $h(0,t)$ as calculated by the FE solution of Eq. (2.2) (solid line) and FD solution of Eq. (4.1) (dashed line). $\alpha = 1$ and $\gamma = 1$ throughout and, from left to right and top to bottom, $\Lambda = 1,\ 3,\ 5,\ 7$ (i.e. $h_0 = 0.148,\ 0.398,\ 0.610,\ 0.797$).

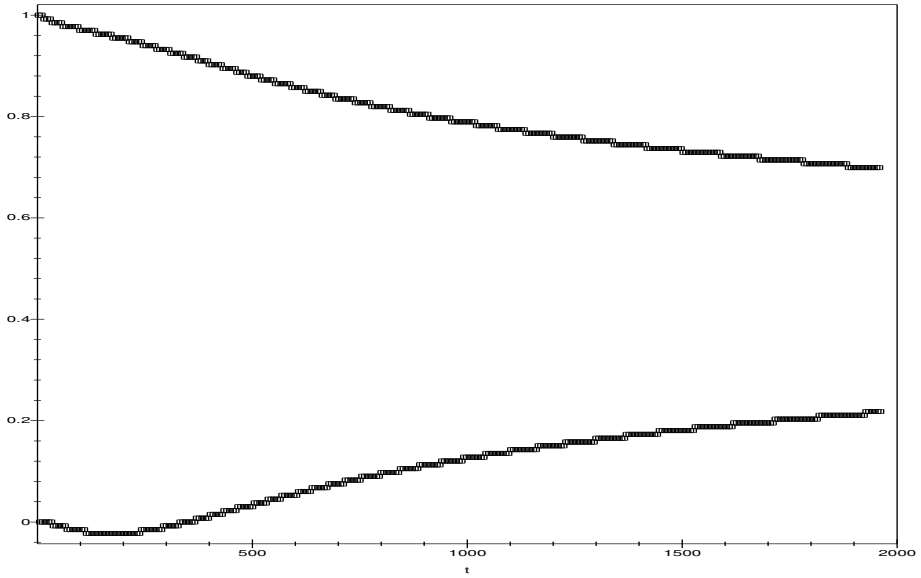

Figure 4. Maximum and minimum values of $h(0,t)$, with $h_0 = 0.112$, from FD solution of lubrication approximation (4.1). Here $\alpha = 1$, $\gamma = 12.5$ and integration is up to $t = 2000$.

a film of uniform thickness is required in the smallest number of roller revolutions possible, the rotation rate should be such that the load is as near as is practically possible to the maximum supportable.

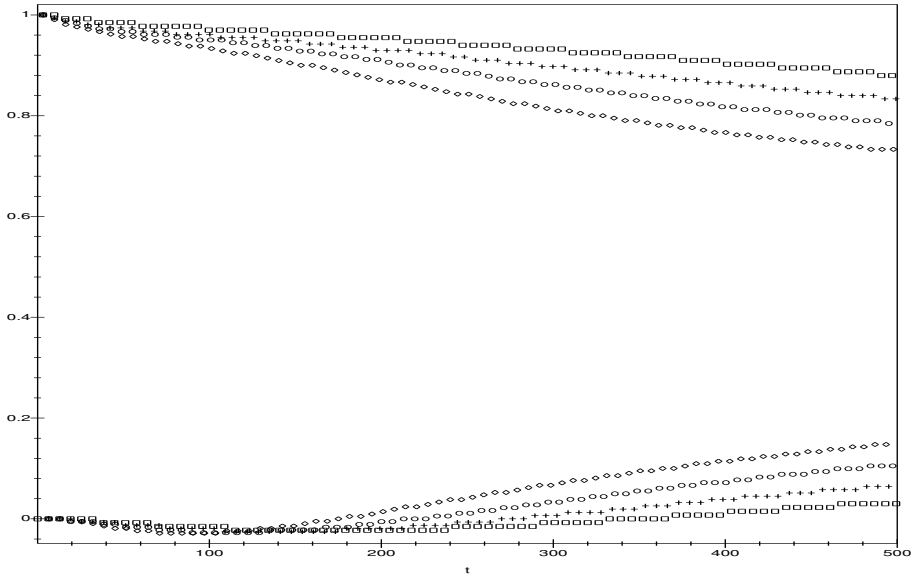

Figure 5. $h(0,t)$ as calculated by FD solution of Eq. (4.1), normalized with respect to first maximum and minimum of oscillation, up to $t = 500$. $\alpha = 1$ and $\gamma = 12.5$. $h(\theta, 0) = 0.110$ ($\Box$), 0.115 ($+$), 0.120 ($\circ$) and 0.125 ($\diamond$).

Figure 6 shows the decay of oscillations to the steady state as a function of the inverse capillary number α. As expected, the higher the surface tension, the more rapidly are subdued the surface oscillations, i.e. the greater the decay rate to the steady state. Note that, when $\alpha = 0.1$, the amplitude of the oscillation first *grows* before decay sets in: this is presumably due to some kind of mode interaction arising through the non-linear nature of (4.1).

Figure 7 shows the decay of oscillations to steady state as a function of the Stokes number γ. It can be seen that, the higher the value of γ, the greater the decay rate to the steady state. It is also seen that, for both $\gamma = 1$ and $\gamma = 5$, no visible decay occurs over this timescale, i.e. $0 \leq t \leq 500$. Indeed, for $\gamma = 5$, large-time calculations reveal that oscillations show first signs of decay at $t = 5000$ whereas one has to integrate beyond $t = 15000$ to see comparable behaviour when $\gamma = 1$.

From the results in this section, it is to be inferred that the precise dynamics of the "delay to decay" are rather intricately dependent upon the initial conditions and physical parameters, leading to physical phenomena occurring over widely disparate time scales. The complex analytical investigation of this aspect lies beyond the scope of the present work.

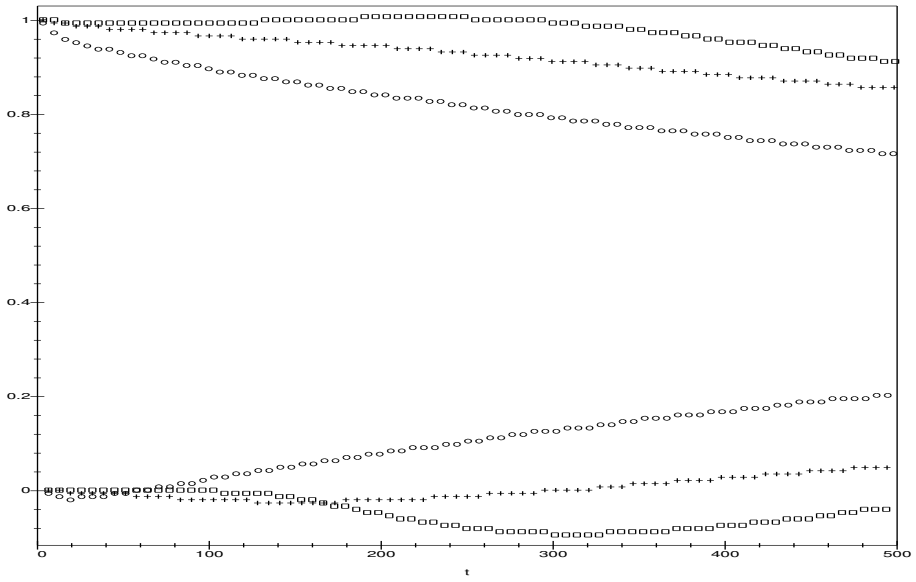

Figure 6. $h(0,t)$ as calculated by FD solution of Eq. (4.1), normalized with respect to first maximum and minimum of oscillation, up to $t = 500$. $h_0 = 0.11298$ and $\gamma = 12.5$. $\alpha = 0.1$ ($\Box$), 1.0 ($+$) and 10.0 ($\circ$).

(*b*) *Unstable flow: load shedding and domain breakup*

Finally, we return to the full Stokes approximation, and our new finite-element method, in order to consider the evolution of unsupportable loads; such flows are characterized by points marked $\Box$ in figure 1. Meshes of fixed connectivity, as are used to investigate stable flows, were unsuitable for unstable flows in which, typically, a bulge develops (see Moffatt 1977) on the free surface during the first rotation of the cylinder which, as it grows, increases the curvature of the free surface considerably until, at some point, the isoparametric discretization fails.

As an example, an initial, unstructured mesh with 64 equally-spaced vertices on each of the free surface and the cylinder was employed, the mesh comprising 520 elements and 2404 unknowns. Parameter values $\Lambda = 5.7$ — a large load — and $\gamma = 1.7$ were selected; figure 8 shows the initial mesh configuration.

Figure 9 shows a series of snapshots leading up to load shedding. Unlike stable flows, there is never symmetry about the line $y = 0$ and a gravity-induced bulge is clearly apparent at $t = 1.95$ which, by $t = 3.95$, has assumed a lobe shape reminiscent of those in the (three-dimensional) experiments of Moffatt (1977): see, in particular, his figure 7. By $t = 10.00$ a curtain, which is clearly going to break from the flow, has started to form. As the simulation continues, the curtain rapidly accelerates in the $\hat{\boldsymbol{\jmath}}$ direction.

In table 2 the increase in the cross-sectional area of the fluid with increasing t is presented. It is readily apparent that, as the simulation of the load shedding evolves, the accuracy — as quantified by the non-mass-conservation error indicator

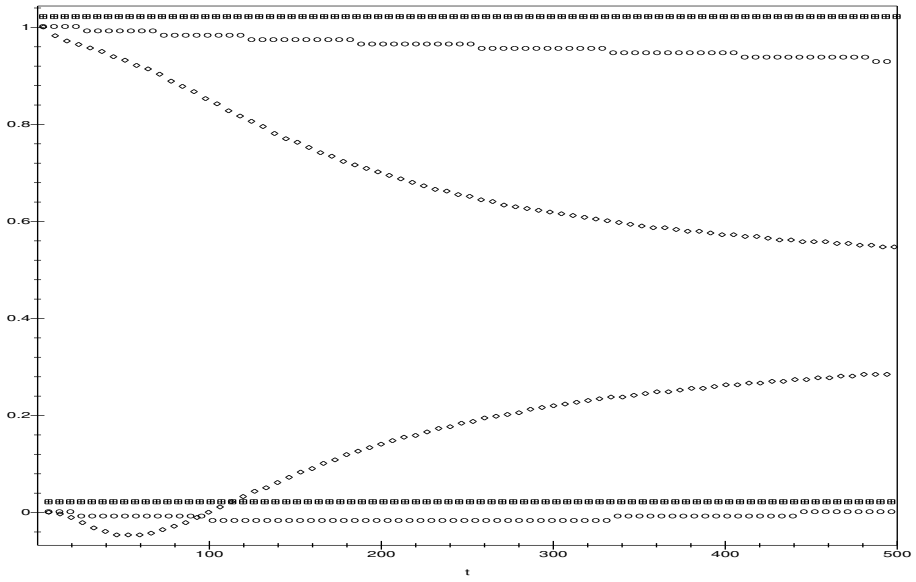

Figure 7. $h(0,t)$ as calculated by FD solution of Eq. (4.1), normalized with respect to first maximum and minimum of oscillation, up to $t = 500$. $h_0 = 0.11298$ and $\alpha = 1$. $\gamma = 1.0$ ($\Box$), 5.0 ($+$), 10.0 ($\circ$) and 20.0 ($\diamond$).

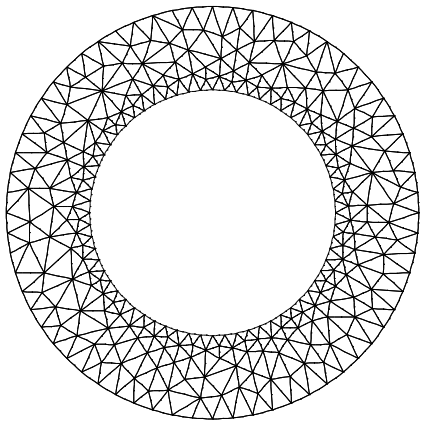

Figure 8. Initial mesh for unstable load-shedding flow; $\Lambda = 5.7$, $\gamma = 1.7$

discussed in § 3 — deteriorates more rapidly in the later stages, and there is therefore little value in extending the calculations any further. The final free-surface profile, at $t = 14.85$, corresponds to the mesh with 839 elements shown in figure 10. This evolution of flow is typical of that observed whenever Λ exceeds the MSL by a moderate amount, irrespective of γ (Peterson 2000).

Two phases of the development of this unstable flow merit discussion in greater

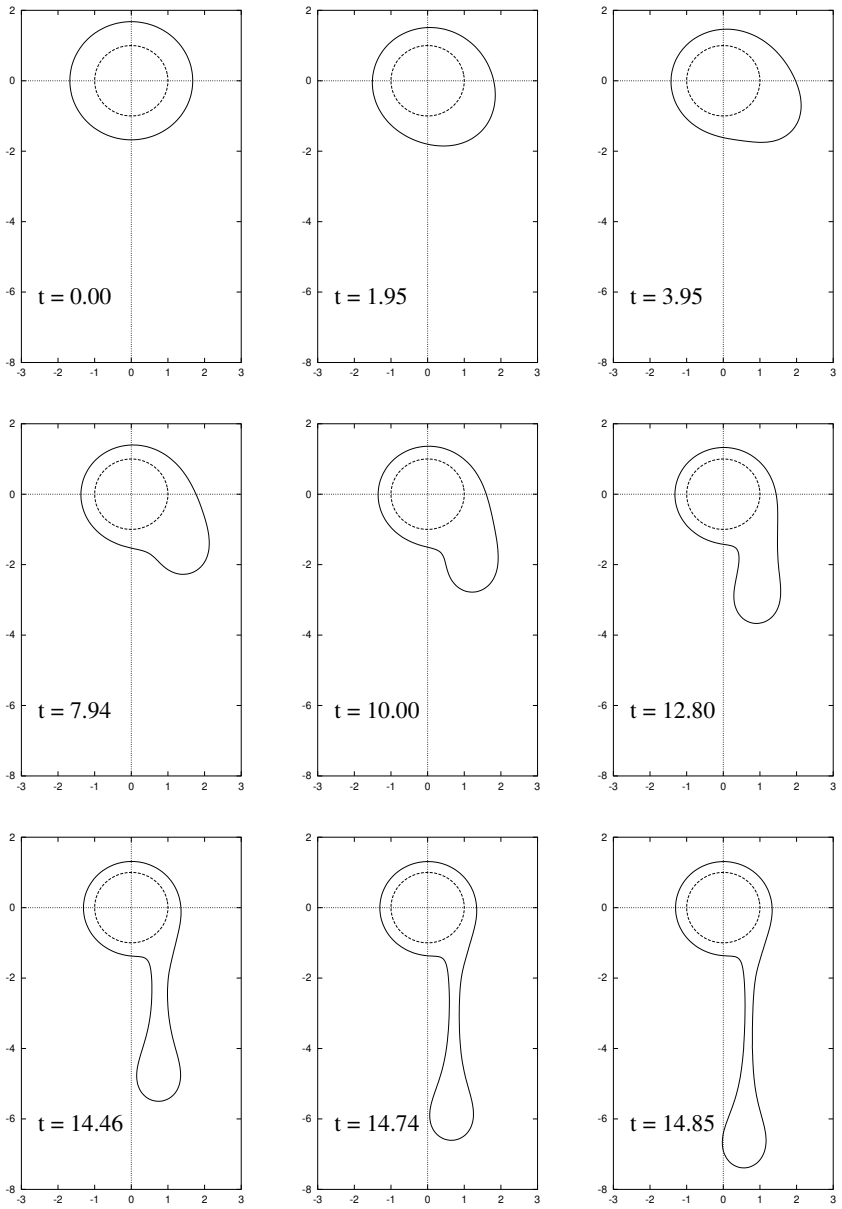

Figure 9. Free surface evolution preceding load shedding; $\Lambda = 5.7$, $\gamma = 1.7$

detail, the first being the development of the lobe. In figure 11, which shows velocity and pressure fields within the lobe at $t = 3.00$, the flow is clearly dominated by viscosity and surface tension effects. By contrast, in figure 12, which shows the velocity and pressure fields within the lobe at $t = 6.95$, we see the first sign of a stagnation point in the lobe, at whose lower end the velocity field is clearly dominated more by the influence of gravity than by the rotating cylinder. Moreover, the pressure field includes a new saddle point where it is attached to the still-rotating

Dimensionless time t	% increase in mesh area
0.00	0.0000
8.00	0.0138
10.00	0.0250
12.80	0.0460
14.46	0.1080
14.74	0.5647
14.86	0.5877

Table 2. *Increase in mesh area during final stages of integration*

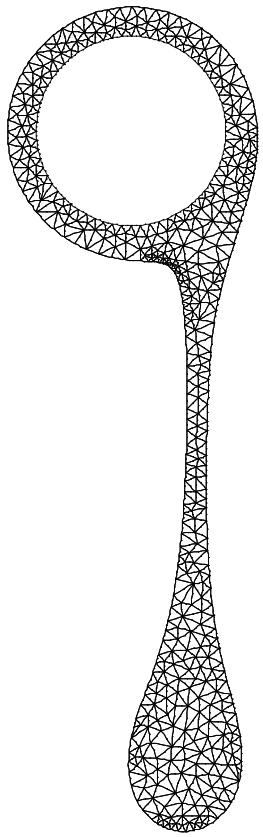

Figure 10. Final mesh ($t = 14.85$) for load-shedding unstable flow; $\Lambda = 5.7$, $\gamma = 1.7$

part of the film. Note that the scalings of the velocity vectors differs between figure 11 and figure 12.

The next interesting phase of the flow occurs around the time the curvature of the downstream side of the lobe changes sign. This phase is illustrated in figures 13 and 14 (in which the different scalings of the velocity field should again be noted),

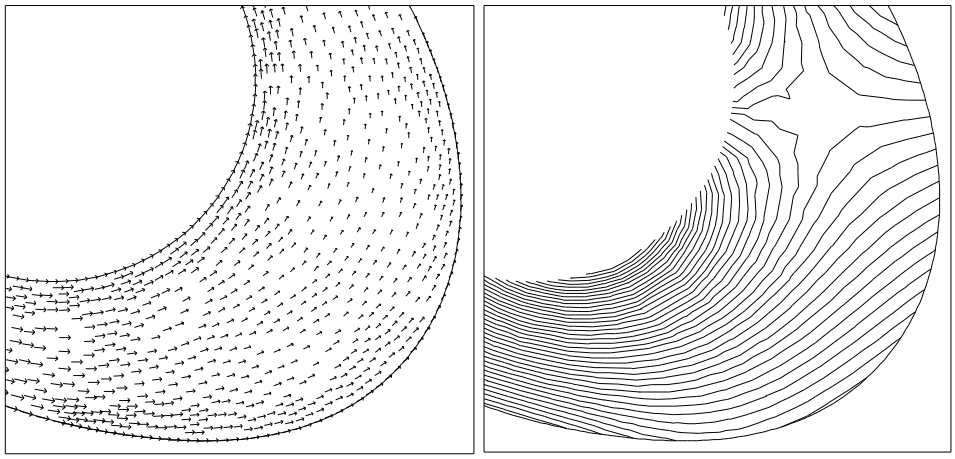

Figure 11. Load-shedding unstable flow, breakdown of near-rigid-body flow, $\Lambda = 5.7$, $\gamma = 1.7$. Velocity and pressure at $t = 3.00$.

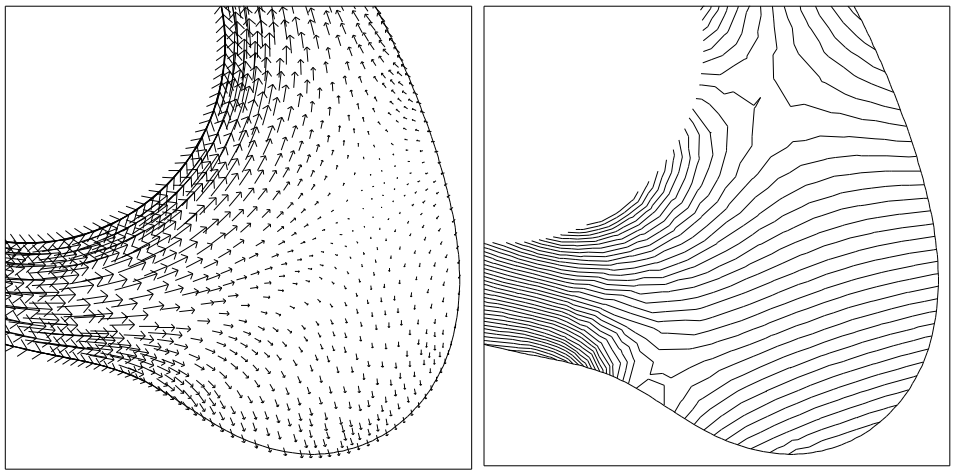

Figure 12. Load-shedding unstable flow, breakdown of near-rigid-body flow, $\Lambda = 5.7$, $\gamma = 1.7$. Velocity and pressure at $t = 6.95$.

in which we note that the near-parallel (with $\hat{\boldsymbol{\imath}}$) pressure contours within the lobe reflect the fact that the flow therein is dominated by the gravity force $-g\hat{\boldsymbol{\jmath}}$.

From $t = 12.80$ onwards the curtain evolves increasingly rapidly under the now-dominant influence of gravity and, as it begins to fall downwards, an elongated neck develops. As this happens, fluid continues to be drawn off from the rotating cylinder and observation suggests that approximately half the initial load will be lost from the cylinder.

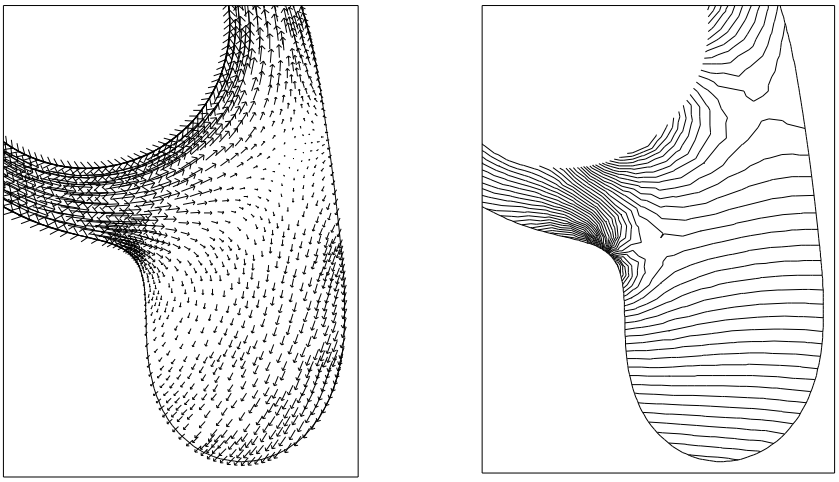

Figure 13. Load shedding problem 2, droplet formation (a) $\Lambda = 5.7$, $\gamma = 1.7$. Velocity and pressure at $t = 11.00$.

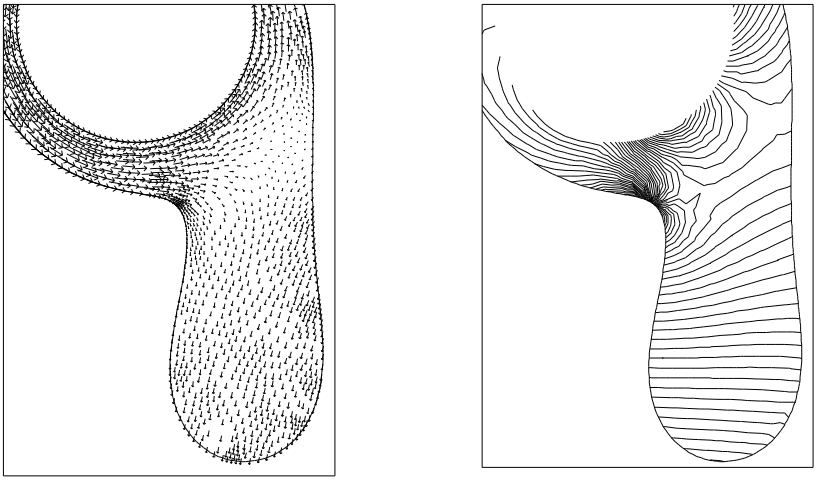

Figure 14. Load shedding problem 2, droplet formation (b) $\Lambda = 5.7$, $\gamma = 1.7$. Velocity and pressure at $t = 12.80$.

5. Conclusions

The time-dependent behaviour of films of viscous fluid supported on a rotating cylinder has been investigated using a Stokes-flow model. While broadly confirming the predictions of the maximum-supportable load made by Moffatt (1977), Hansen & Kelmanson (1994) and Kelmanson (1995), the computations reported here suggest that, even for those regions of the $\{\Lambda, \gamma\}$ parameter space in which convergence (from an arbitrary initial configuration) towards a stable, steady state is expected, the rate of convergence decreases with the initial mean film height, the surface tension and the gravitational force. Indeed, a complex dependence of solutions — occurring over widely disparate time scales — upon these parameters has

been demonstrated, and this is the subject of ongoing asymptotic analyses which lie outside the scope of this paper.

Our adaptive-finite-element Stokes solver has enabled preliminary studies to be undertaken regarding the range of validity of the thin-film approximation for a variety of flow parameters; it would appear that the lubrication approximation can be made increasingly more valid, as the film thickness increases, by either decreasing the gravitational field or increasing the rate of rotation of the cylinder. Finally, new results illustrating the phenomenon of load shedding — whose dynamics lie beyond the demonstrated range of validity of the lubrication approximation — are presented.

The authors wish to express their sincere gratitude to Professor E J Hinch, FRS, for suggesting numerous and diverse improvements to the first draft of this paper; in particular, for detailed considerations regarding the numerical investigation of decay rates using a lubrication approximation. Comments of a second referee are also acknowledged. RCP gratefully acknowledges receipt of joint financial support from the School of Computing and Department of Applied Mathematics of the University of Leeds.

References

Ashby, S.F., Manteuffel, T.A. & Saylor, P.E. 1990 A taxonomy for conjugate gradient methods, *SIAM J. Num. Anal.* **27(6)**, 1542–1568.

Campanella, O.H. & Cerro, R.L. 1984 Viscous flow on the outside of a horizontal rotating cylinder: the roll-coating regime with a single fluid, *Chem. Engng. Sci.* **39**, 1443–1449.

Ciarlet, P.G. 1978 *The Finite Element Method for Elliptic Problems*, Studies in Mathematics and its Applications, Vol.4, North-Holland Publishing Company.

Duffy, B.R. & Wilson, S.K. 1999 Thin film and curtain flows on the outside of a rotating horizontal cylinder, *J. Fluid Mech.* **394**, 29–49.

Gresho, P.M. 1991 Incompressible fluid dynamics: some fundamental formulation issues, *Ann. Rev. Fluid Mech.* **23**, 413–453.

Gunzburger, M.D. 1989 *Finite Element Methods for Viscous Incompressible Flows*, Academic Press, San Diego, California.

Hansen, E.B. & Kelmanson, M.A. 1994 Steady, viscous, free-surface flow on a rotating cylinder. *J. Fluid Mech.* **272**, 91–107.

Hosoi, A.E. & Mahadevan, L. 1999 Axial instability of a free surface from in a partially filled horizontal rotating cylinder, *Phy. Fluids* **11**, 97–106

Johnson, R.E. 1988 Steady-state coating flows inside a rotating horizontal cylinder, *J. Fluid Mech.* **190**, 321–342.

Johnson, R.E. 1990, Coating flow stability in rotational molding. In *Engineering Science, Fluid Dynamics: A Symposium to Honor T Y Wu* (ed. G T Yates), pp.435–449. World Scientific.

Joseph, D.D. & Preziosi, L. 1987 Stability of rigid motions and coating films in bicomponent flows of immiscible liquids, *J. Fluid Mech.* **185**, 323–351.

Kelmanson, M.A. 1995 Theoretical and experimental analyses of the maximum-supportable fluid load on a rotating cylinder. *J. Engng Math.* **29**, 271–285.

Lynch, D.R. 1982 Unified approach to simulation on deforming elements with application to phase-change problems. *J. Comput. Phys.* **47**, 387–411.

Melo, F. 1993 Localised states in a film-dragging experiment, *Phys. Rev. E* **48(4)**, 2704–2712.

Moffatt, H.K. 1977 Behaviour of a viscous film on the outer surface of a rotating cylinder. *J. Méc.* **187**, 651–673.

Oron, A., Davis, S.H. & Bankoff, S.G. 1997 Long-scale evolution of thin films, *Rev. Mod. Phys.* **69(3)**, 931–980.

Peterson, R.C. 2000 The numerical solution of free-surface problems for incompressible, newtonian fluids. Ph.D. thesis, University of Leeds, U.K.

Peterson, R.C., Jimack, P.K. & Kelmanson, M.A. 1998 Automatic generation of finite-element meshes for evolving gas/liquid interfaces with arbitrary geometry. In *Proceedings of the 6th ICFD Conference on Numerical Methods in Fluids*, Oxford, U.K., 467–473.

Peterson, R.C., Jimack, P.K. & Kelmanson, M.A. 1999 The solution of two-dimensional free-surface problems using automatic mesh generation. *Int. J. Num. Meth. Fluids* **31**, 937–960.

Preziosi L. & Joseph, D.D. 1988 The run-off condition for coating and rimming flows. *J. Fluid Mech.* **272**, 99–113.

Pukhnachev, V.V. 1977 Motion of a liquid film on the surface of a rotating cylinder in a gravitational field. *Z. Prikl. Mekh. i Tekh. Fiz.* **3**, 78–88. (Transl. 1977 *J. Appl. Mech. Tech. Phys.* **18**, 344–351.)

Ramage, A. & Wathen, A.J. 1994 Iterative solution techniques for the Stokes and Navier-Stokes Equations, *Int. J. Num. Meth. Fluids* **19**, 67–83.

Saad, Y. 1996 ILUM: A multi-elimination ILU preconditioner for general sparse matrices, *SIAM J. Sci. Comp.* **17(4)**, 830–847.

Shewchuk, J.R. 1996 *Triangle: Engineering a 2D Quality Mesh Generator and Delaunay Triangulator*, Proceedings of the First workshop on Applied Computational Geometry, Philadelphia, Pennsylvania, 123–133.

Strang, G. & Fix, G.J. 1973 *An Analysis of the Finite Element Method*, Prentice-Hall, New Jersey.

Weidner, D.E., Schwartz, L.W. & Eres, M.H. 1997 Simulation of coating layer evolution and drop formation on horizontal cylinders, *J. Coll. Interf. Sci.* **187**, 243–258.

Wilson, S.D.R. & Williams, J. 1997 The flow of a liquid film on the inside of a rotating cylinder, and some related problems, *Phys. Fluids* **9**, 2184–2190.